Supplement of Hydrol. Earth Syst. Sci., 27, 401–415, 2023
https://doi.org/10.5194/hess-27-401-2023-supplement
© Author(s) 2023. CC BY 4.0 License.

Hydrology and Earth System Sciences
Open Access
EGU

*Supplement of*

# The origin of hydrological responses following earthquakes in a confined aquifer: insight from water level, flow rate, and temperature observations

**Shouchuan Zhang et al.**

*Correspondence to:* Zheming Shi (szm@cugb.edu.cn)

The copyright of individual parts of the supplement might differ from the article licence.

**Contents of this file**



**S1. Aquifer lithology and wellbore structure of Dazhai deep well aquifer system**:

The lithology of the wellbore in Dazhai deep well is as follow (Figure S1): 0m~22.43m is quaternary deposit, 22.43m~71.97m is silty mudstone, 71.97m~105m is detrital sandstone with fissure developed, 105m~117.37m is mudstone, 117.37m~191.10m is detrital sandstone with fissure developed, 191.10m~196.97m is mudstone, 196.97m~401.28m is thick bedded mudstone, and 401.28m~410.31m is detrital sandstone.

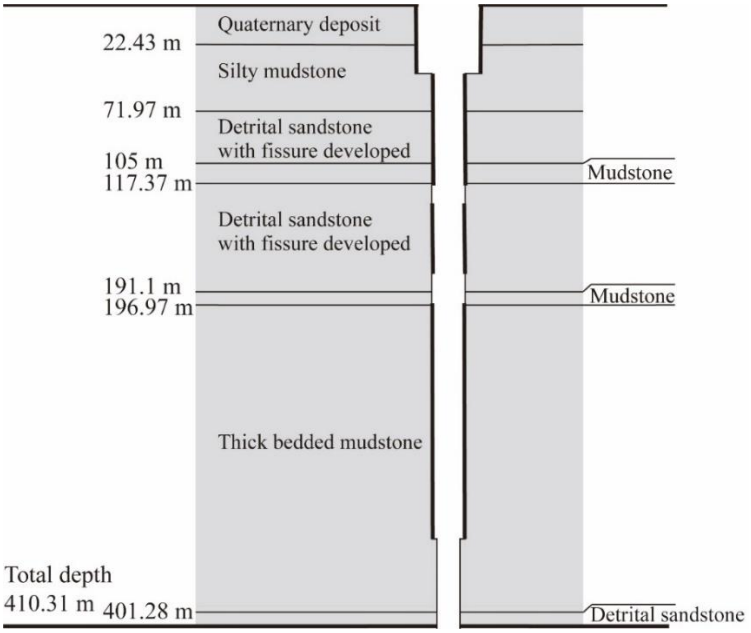


Figure S1. Aquifer lithology and wellbore structure of Dazhai deep well aquifer system.

**S2. The raw data of water level in Dazhai well:**

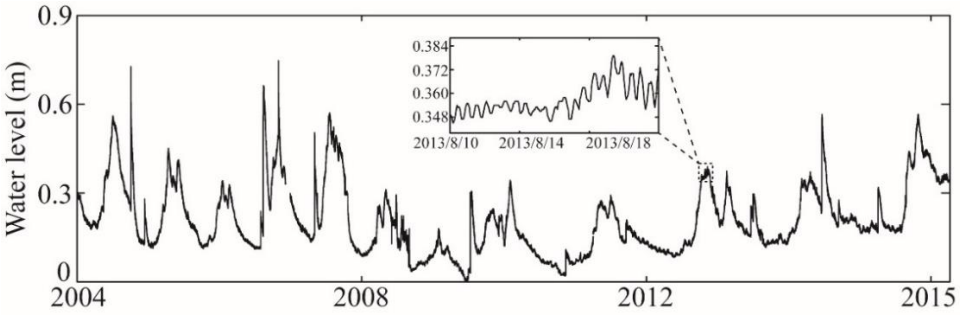


Figure S2. The raw data of water level in Dazhai well. The inset represents the zoom-in of the time series.

The raw data of water level is shown in Figure S2, and the inset is that the water level in Dazhai well shows responds to Earth tides.

**S3. The effect of air temperature on the variation of water temperature:**

Wavelet coherence is employed to analyze the correlation between water temperature and air temperature in time domain and frequency domain. Taking EQ1 as an example to analyze. The result of wavelet coherence indicates that there is no correlation between water temperature and air temperature. In addition, the temperature probe is located about 100m below the water surface, which is helpful for removing the influence of air temperature on the variation of water temperature. Thus, air temperature fluctuation would not have effect on the variation of water temperature.

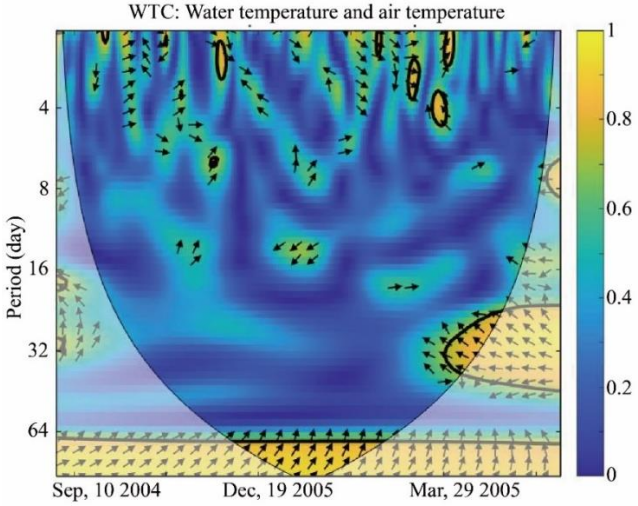


Figure S3. Wavelet coherence between water temperature and air temperature. The thick black contour specifies the 95% confidence level. The arrow directions indicate the relative phase relationship: in-phase pointing right, antiphase pointing left, and phase-leading by 90° pointing straight down.

## S4. The seismic energy density of earthquakes

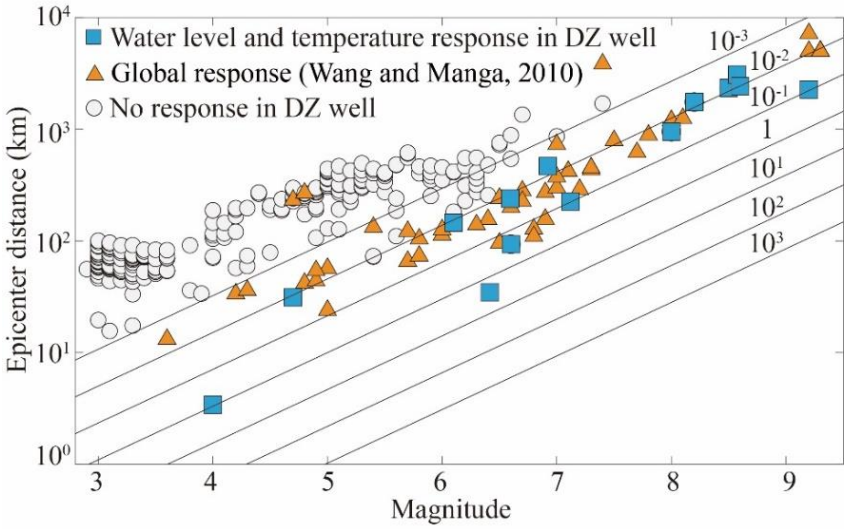


Figure S4. Distribution of earthquake-triggered hydrologic changes as a function of earthquake magnitude and distance. Orange triangles represent earthquakes with hydrological response collected from Wang and Manga (2010). Blue squares represent 14 earthquakes of this study that induce hydrological response in DZ well. White circles represent earthquakes without hydrological response in DZ well.

## S5. Spectral analysis of water level in Dazhai well:

The obvious amplitudes were observed in a frequency band of 0~3cpd (Figure S3), indicating that the water level in Dazhai well responds to Earth tides.

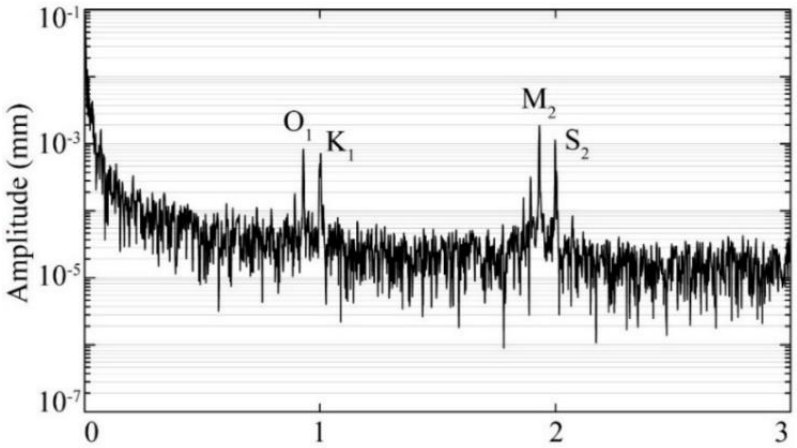


Figure S5. Amplitude spectrum for hourly water levels in Dazhai Well, western Yunnan Province, China.

## S6. The effect of barometric pressure on the variation of water level.

In order to identify the effect of barometric pressure on the variation of water level in Dazhai well, the wavelet coherence is employed to explore the correlation between water level and barometric pressure, and

then the tidal components of water level in Dazhai well extracted from the variation of water level is compared under and without the influence of barometric pressure. Taking EQ1 as an example to analyze. The hourly monitoring data of water level and barometric pressure from Sep, 1 2004 to May, 30 2005 are chosen for the wavelet coherence analysis and extracting the tidal components.

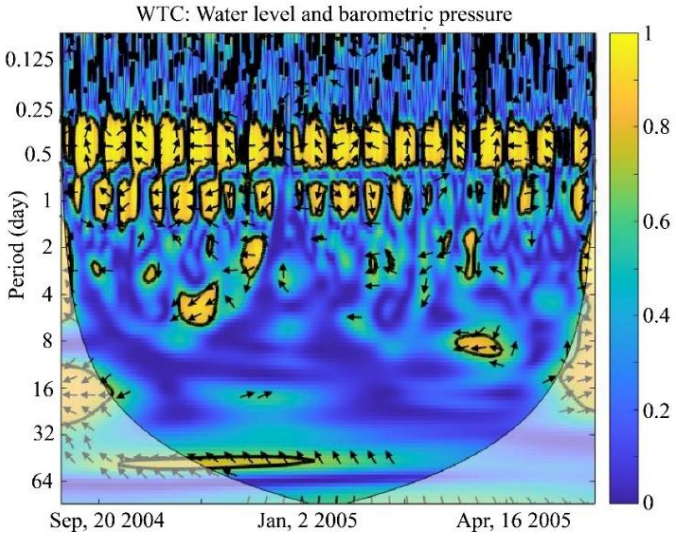


Figure S6. Wavelet coherence between water level and barometric pressure. The thick black contour specifies the 95% confidence level. The arrow directions indicate the relative phase relationship: in-phase pointing right, antiphase pointing left, and phase-leading by 90° pointing straight down.

The wavelet coherence is used to explore water level response to barometric pressure, which is a powerful tool to analyzing nonstationary signals. We convert the time series of water level and barometric pressure into time-frequency space based on the wavelet coherence. In Figure R1, the water level and barometric pressure are highly correlated at a 95% pointwise confidence level with coherence coefficients > 0.9 within band between 0.5 and 1 day. The semidiurnal period is evident throughout the entire data set. Periods of approximately 1 day are slightly unstable. The result of wavelet analysis indicates that the variation of water level is affected by barometric pressure.

We compare the tidal components extracted from the water level time series under and without the influence of barometric pressure. Baytap-G program is used to remove the interference caused by barometric pressure in the time series of water level (Tamura et al., 1991). The mathematical theory in Baytap-G program supposes that the time series can be divided into several items, as follow:

$$y_i = \sum_{m=1}^{M} \left( \alpha_m C_{mi} + \beta_m S_{mi} \right) + \sum_{k=0}^{K} b_k x_{i-k} + d_i + e_i \tag{R1}$$

Where the first term and second term on the right-hand side represent the tidal components and barometric pressure components, respectively; $d_i$ is the long-time drift; and $e_i$ is the random noise. By using Baytap-G program, the tidal components are extracted from the water level time series with the elimination of barometric pressure (Figure R2). Compared the tidal components extracted from the water level time series under and without the influence of barometric pressure (Figure S7 and S8), the results are similar and it is

indicated the effect of barometric pressure on the variation of water level has little effect on the extraction of tidal components from the water level time series.

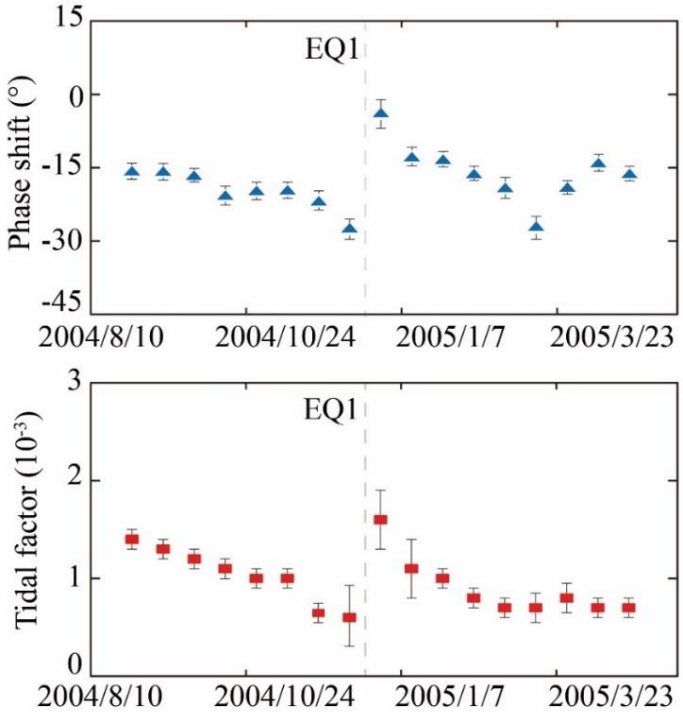


Figure S7. Tidal analysis without removing barometric pressure by Baytap-G (a) Amplitude ratio and (b) Phase shift. The gray dash line indicates the time the earthquake occurred.

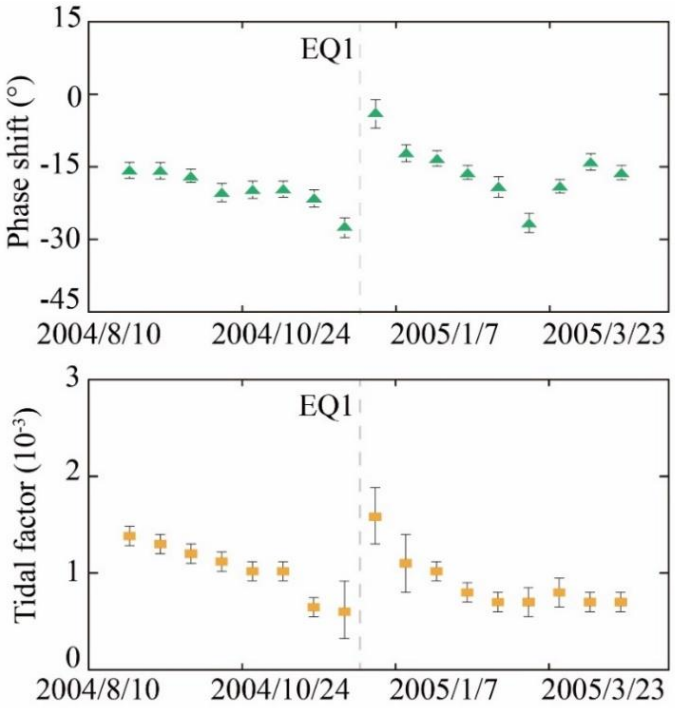


Figure S8. Tidal analysis after removing barometric pressure by Baytap-G (a) Amplitude ratio and (b) Phase shift. The gray dash line indicates the time the earthquake occurred.

**S7. The flow chart of different mechanisms and methods.**

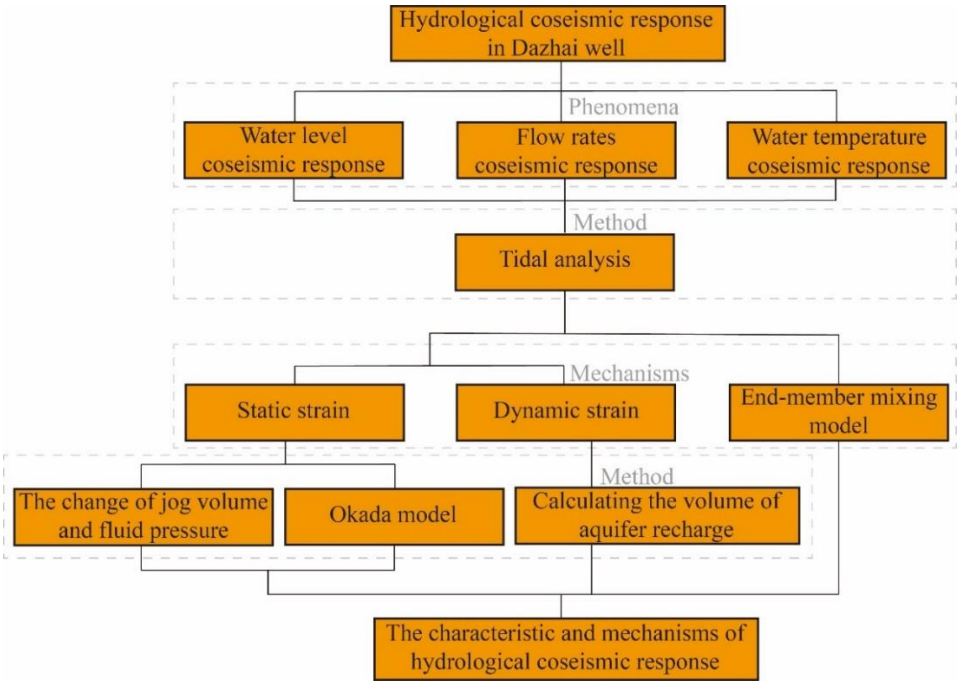


Figure S9. The flow chart.

**S8. Fault-plane solutions for earthquakes**

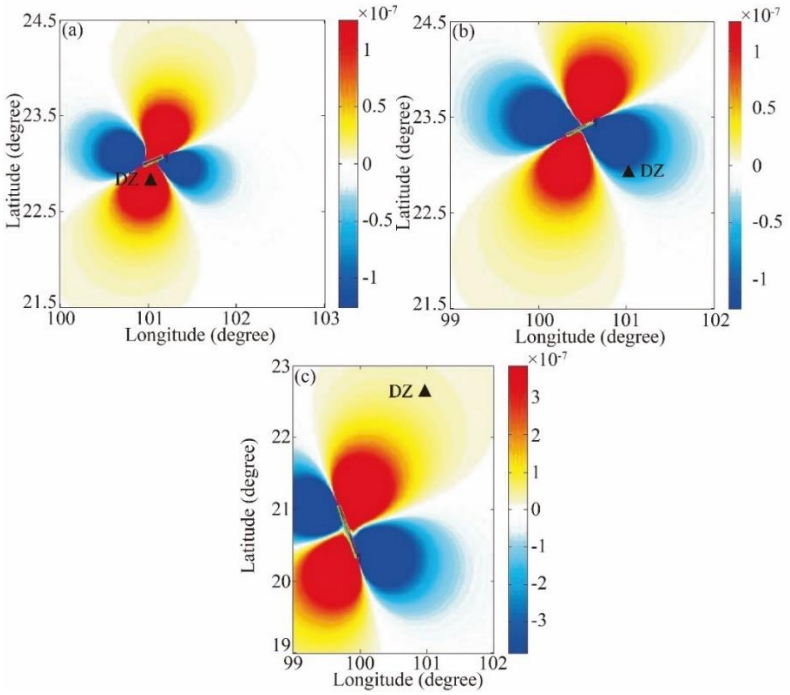


Figure S10. Coseismic static strain caused by (a) EQ4 *Mw* 6.4 2007/6/3, (b) EQ12 *Mw* 6.6 2014/10/7, and (c) EQ7 *Mw* 7.2 2011/3/24. Blue zones show contraction while the red zones indicate dilation. Location of Dazhai Well (DZ) indicated using black triangle.

Table S1. Fault-plane solutions for four earthquakes examined in this study.

| Earthquake ID | Date | Hypocentral depth (km) | Strike (°) | Dip (°) | Rake (°) |
|---|---|---|---|---|---|
| EQ4 | Jun, 3 2007 | 5 | 247 | 69 | 30 |
| EQ6 | May, 12 2008 | 19 | 222 | 29 | 152 |
| EQ7 | Mar, 24 2011 | 8 | 340 | 77 | 176 |
| EQ12 | Oct, 7 2014 | 8.5 | 242 | 79 | -7 |

**S9. The accuracy and efficiency of model fitting results**

Three error metrics are conducted to evaluate the accuracy and efficiency of model fitting results, as follow:

Root mean square error (RMSE):

$$\mathrm{RMSE} = \sqrt{\frac{\sum_{i=1}^{N}(y_i - y_i^*)^2}{N}} \tag{S1}$$

The Nash-Sutcliffe efficiency (NSE):

$$\mathrm{NSE} = 1 - \frac{\sum_{i=1}^{N}(y_i - y_i^*)^2}{\sum_{i=1}^{N}(y_i - \bar{y}_i)^2} \tag{S2}$$

The coefficient of determination:

$$R^2 = 1 - \frac{\sum_{i=1}^{N}(y_i - y_i^*)^2}{\sum_{i=1}^{N} y_i^2 - \frac{\sum_{i=1}^{N} y_i^{*2}}{N}} \tag{S3}$$

where $y_i$ is the observed value, $y_i^*$ are the simulated value, $\bar{y}_i$ is the mean of observed values and N the number of observations. The RMSE is the deviation between the observed and simulated values, and smaller values indicate a better model. NSE measures the model performance for training and testing, which is an efficiency indicator for hydrologic models. The value of NSE close to 1 represents the model predictability is satisfactory (Yoon et al., 2011). $R^2$ is used to analyze the linear regression goodness of fit between observed and simulated value. When RMSE is close to 0, and NSE and $R^2$ are close to 1, this model is regarded as a good fit between simulated and observed value.

The scatter plot of the fitted and observed value is shown in Figure S5. The X-axis and Y-axis represent the observed value and simulated value respectively. Under the ideal condition, the prediction results should be distributed over X=Y or evenly distributed on both sides of the line. The closer the point to the X=Y line, the smaller the errors. The model fitted errors are summarized in Table S2. The RMSE of all models range from 0.04 to 0.06, the NSE value ranges from 0.83 to 0.98, and the $R^2$ are greater than 0.84. Although the fitting results are not such perfect at the maximum value of discharge after earthquakes, the error analysis

show that the errors evaluated by different methods are small and acceptable. Thus, we consider that our model is able to describe the co-seismic discharge processes following the different earthquakes.

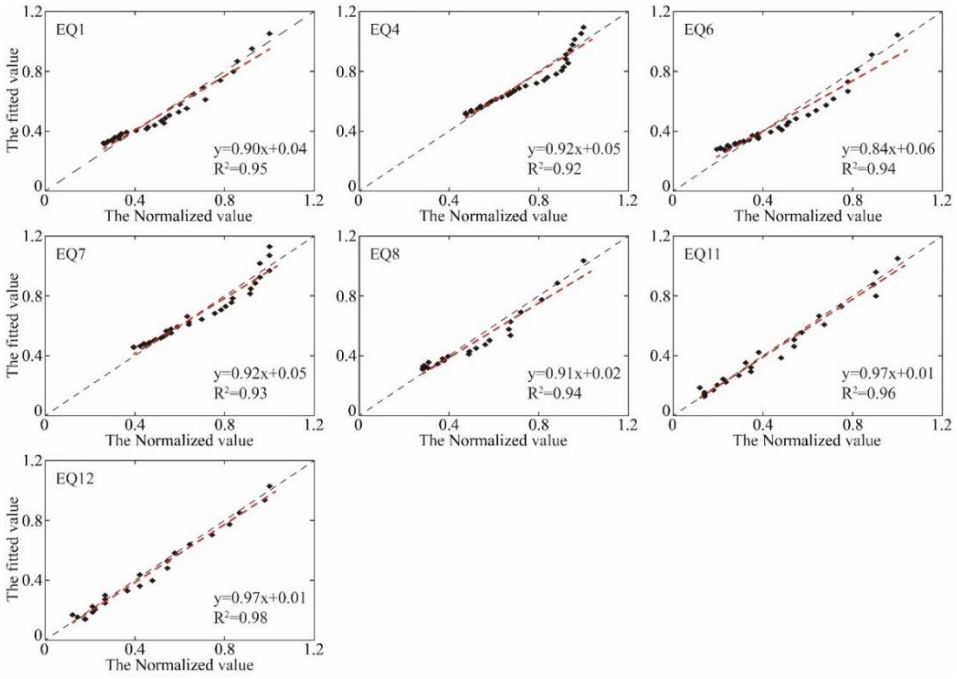


Figure S11. Scatter plot of the simulated and observed value. Gray dotted lines represent 1:1 line. The red solid lines dashed line represents the trend lines.

Table S2. The models fitting errors following seven earthquakes.

| Earthquake ID | Date | RMSE | NSE | $R^2$ |
|---|---|---|---|---|
| EQ1 | Dec, 26 2004 | 0.05 | 0.97 | 0.95 |
| EQ4 | Jun, 3 2007 | 0.05 | 0.98 | 0.92 |
| EQ6 | May, 12 2008 | 0.06 | 0.96 | 0.94 |
| EQ7 | Mar, 24 2011 | 0.05 | 0.98 | 0.93 |
| EQ8 | Apr, 11 2012 | 0.06 | 0.97 | 0.94 |
| EQ11 | Feb, 5 2014 | 0.05 | 0.95 | 0.96 |
| EQ12 | Oct, 7 2014 | 0.04 | 0.98 | 0.98 |

## S10. The results of wavelet coherence analysis.

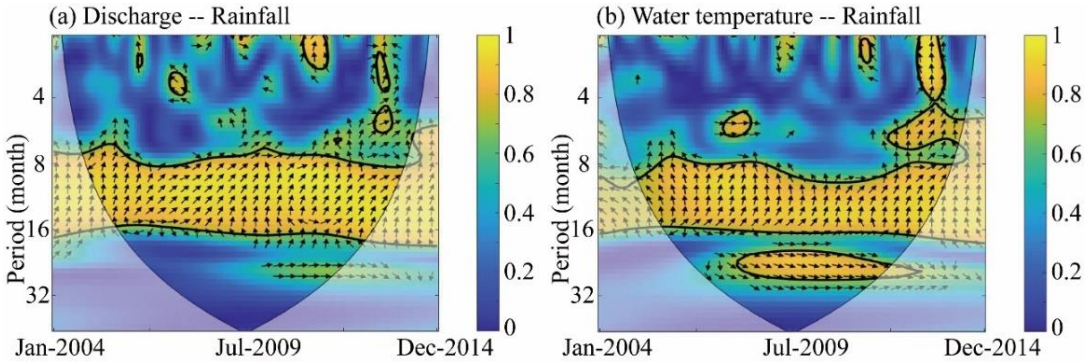


Figure S12. Wavelet coherence analysis between (a) discharge and rainfall (b) water temperature and rainfall. Thick black contour indicates the 95% confidence level and lighter shade indicates regions inside the cone of influence (COI). Arrows indicate the relative phase relationship (in-phase pointing right, anti-phase pointing left, and phase-leading by 90° pointing down).

**References:**

Yoon, H., Jun, S.-C., Hyun, Y., and Gwang-Ok: A comparative study of artificial neural networks and support vector machines for predicting groundwater levels in a coastal aquifer, Journal of Hydrology, 396, 128-138, https://doi.org/10.1016/j.jhydrol.2010.11.002, 2011.